CHARACTERIZATION OF ZIRCONIUM SUBSTITUTED COBALT ZINC FERRITES SYNTHESIZED VIA Co-PRECIPITATION TECHNIQUE

M. S. SHIFA[a], A.MISBAH [a], T. MUNIR[a], A. SHAHZAD[a], M. N. USMANI[d], M. KHALID[b], S. MUTABAR [e], Q. IMDADULLAH [c], Z. A. GILANI[b*], H. M. N. UL HUDA KHAN ASGHAR[b]

[a]*Nanoferrites Synthesis & Texture Analysis Lab, Department of Physics, Government College University Faisalabad, Pakistan*

[b]*Department of Physics, University of Information Technology, Engineering &Management Sciences, Quetta, Pakistan*

[c]*Department of Chemistry, University of Science and Technology Bannu, Khyber Pakutunkhwa, Pakistan*

[d]*Department of Physics, Bahauddin Zakariya University, Multan, Pakistan.*

[e]*Department of Physics, University of Peshawar, Pakistan*

This present work express the effect of zirconium substitution on the properties of the CoZn spinel properties prepared via co-precipitation method. X-ray diffraction, Fourier transform infrared spectroscopy (FTIR), Scanning electron spectroscopy (SEM) and magnetic properties are employed with different concentration $Co_{0.5}Zn_{0.5}Zr_xFe_{2-x}O_4$; x = 0.0, 0.2, 0.4, 0.6, 0.8, 1.0 where the effect of substitution on the structure, optical, surface morphology and magnetic parameters were studied. Particle size ranging 12nm to 48nm was calculated from XRD data. Moreover formation of the single phase spinel ferrites is also confirmed. Using a vibrating sample magnetometer (VSM), saturation magnetization and coercivity are measured in the range of -2000Oe to 2000Oe.Saturation magnetization 'Ms' was enhanced to 52emu/g where as maximum coercivity 'Hc' values (144.14Oe) have been obtained. The value of Hc is low, so in soft ferrite range. Hence synthesized $Co_{0.5}Zn_{0.5}Zr_xFe_{2-x}O_4$ferrites are suitable for electromagnetic induction.

(Received January 16, 2019; Accepted July 25, 2019)

Keywords: Zirconium, Nanocrystalline ferrites, XRD, SEM, FTIR, Co-Precipitation, Magnetic properties

1. Introduction

Nanotechnology has gain interest of researchers and material scientists due to versatile physical and chemical properties of nanomaterials. Nanoparticles also had been extensively studied in recent years. These particles consist of number of atoms or molecules bonded together having radius less than 100nm. So, a nanoparticle has the size approximately equal to 10^{-9}m or 10Å[1]. The ferrites (magnetic oxides) have been used in many applications for several years ago. Magnetic materials are present in the form of hard and soft ferrites. Hard ferrites are permanent magnetic materials while soft ferrites are temporary magnetic materials. Both types have plenty of applications in electrical and electronics industry[2].Spinel ferrite nanoparticles are mostly studied by researcher now a day because they are technologically very important materials. They have many remarkable structural, electric, optical and magnetic properties[3]. Their properties make them suitable in various fields like high-frequency systems, electronic circuits and power delivering devices. These ferrites have high electrical resistivity and low eddy current losses. Spinel ferrites have general form AB_2O_4 (A-site and B-site) [4]. This formula can also be symbolized as $(A_{1-x}B_x)_{tetra}[A_xB_{2-x}]_{octa}O_4$. These ferrites have cubic structure. The general form for cubic spinel ferrites is written as $MeFe_2O_4$, here Mere present a divalent metal ion such as Cd^{2+}, Cu^{2+}, Fe^{2+} and Ni^{2+}. The spinel ferrites structure is actually the arrangement of oxygen ions or

*Corresponding author: zagilani2002@yahoo.com

anion in the lattice [5, 6].They have wide range of applications. The low conductivity of ferrite nanoparticles make them suitable for microwave applications. These magnetic materials are extensively used in magnetic fluids, permanent magnets, audio-video tapes, digital recording, disk recording, magnetic refrigeration system, density storage devices, memory cores of computers, bubble devices, microwave devices, transformers, electric generators, ultrasonic generators, moderators, phase shift, isolators and satellite communication [7]. Ferrites are also used in telephone exchange, computers, and control equipment. Choice of better synthesis method will lead to get good quality ferrites. Ferrites allow metal cations to occupy different sites. This will enable them to change their electrical and magnetic properties. So, that we can use them in electronics and microwave industry [1, 8].

The properties of cobalt ferrites can be further improved by substitution of metal ions with suitable variation. When cobalt ferrites are substituted by different metal ions, the interactions between Co^{2+} and Fe^{3+} ions at A and B sites may occur. Due these interactions, many profitable electrical and magnetic properties achieved. Distribution of various cations at octahedral and tetrahedral sites will lead to modification their properties [9-12].

2. Experimental details

A series with general formula $Co_{0.5}Zn_{0.5}Zr_xFe_{2-x}O_4$ with composition variation x = 0.00, 0.20, 0.40, 0.60, 0.80, 1.00 of soft or spinel ferrites was prepared by chemical co-precipitation route. Many authors used co-precipitation technique to fabricate ferrite nanoparticles [13]. Here we used it to fabricate the Zr ion substituted soft ferrite nanoparticles $Co_{0.5}Zn_{0.5}Zr_xFe_{2-x}O_4$ (x = 0.00, 0.20, 0.40, 0.60, 0.80 and 1.00). Raw materials were zinc chloride ($ZnCl_2$), ferric nitrate or Iron (III) nitrate (Nona hydrate) having chemical formula $Fe(NO_3)_3.9H_2O$, cobalt nitrate (hexahydrate) having chemical formula $Co(NO_3)_2.6H_2O$ and zirconium (IV) oxychloride $ZrOCl_2.8H_2O$ and ammonia solution. All these chemicals (metal chlorides and nitrates) are soluble in deionized water. First we collected five beakers of 1000 milliliter (ml). We dissolved metal nitrate in deionized water as cobalt nitrate solution (29.1/1000ml), Zinc chloride solution (13.6/1000ml), ferric nitrate solution (80.8/1000ml) and zirconium oxychloride solution (32.2/1000ml). For the preparation of first sample $Co_{0.5}Zn_{0.5}Fe_2O_4$ (x = 0.00), the mixed solutions of cobalt nitrate, zinc chloride and ferric nitrate in their respective stoichiometry (100 ml of 0.1M cobalt nitrate, 100 ml of 0.1M zinc chloride and 200 ml of 0.2M ferric chloride) were prepared and so on. These homogeneous solutions were then kept on hot plate. They were continuously stirred and raise the temperature of hotplate 50 to 60°C. When these solutions attained this temperature, we maintain their pH value up to 11. The precipitates were formed in the bottom of glass beakers. These precipitates can be seen by necked eye. But these precipitates also contained nitrate and chloride ions. These nitrates and chlorides are unwanted. These were removed by washing the precipitates many times. The precipitates were filtered and washed thoroughly with deionized water until the precipitates were free from water soluble impurities and it became neutral. The product was then dried by using electric thermostatic drying oven at 95°C until all water contents removed. The dried precipitates were mixed homogeneously in an agate mortar and pestle for 30 minutes. The fine powders were obtained. This fine powder were again heated at 700°C for 6 hours by using furnace and then cooled slowly. The heated products again grind into fine powder with the help of mortar pestle. These fine powders were saved in sample holder tubes and used required volume for characterization.

3. Discussions

3.1. XRD analysis

X-ray powder diffraction (XRD) patterns were gained by using Netherlands, X' Pert Pro PAN Analytical X-ray diffractometer with Cu Kα=1.54Å. The X-ray diffraction analysis was done for prepared samples $Co_{0.5}Zn_{0.5}Zr_xFe_{2-x}O_4$ (x = 0.0, 0.2, 0.4, 0.6, 0.8, 1.0). In order to get the information about the phases developed in the prepared samples, all samples were scanned for 15°

to 65° at 2θ. X-ray diffraction is one of the best nondestructive technique use to study the crystalline nature of material. Each material have specific pattern because of distinct crystalline lattice parameter and different packing of molecules[14].

The diffraction patterns for these ferrite nanoparticles were depicted in the Fig.1. The broader peaks in XRD pattern showed that the particles were in Nano size. XRD data confirmed the presence of spinel phase in all prepared samples.

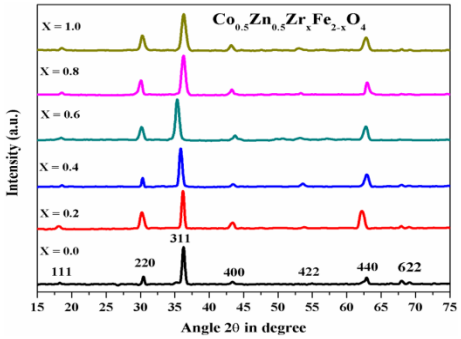

Fig. 1.XRD patterns of "$Co_{0.5}Zn_{0.5}Zr_xFe_{2-x}O_4$" spinel ferrite (x = 0.0 to 1.0).

Typical peaks of spinel ferrites were seen for each sample. The six dominant peaks were observed at 2θ= 18°, 30°, 35°, 43°, 53° and 62°. These intense X-ray diffraction peaks corresponds to the planes (111), (220), (311), (400), (422) and (440) are indication of the formation of spinel ferrite phase and these angles and hkl values are compared with JCPDS (ICCD#00-008–0234) data card [15]. There are some minute peaks; may be due the presence of impurities in the raw material. All the diffraction peaks are well indexed with the previous published papers of zirconium substituted spinel ferrites [16, 17].

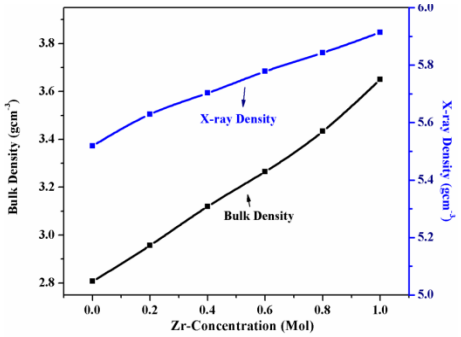

Fig. 2. The variation in bulk density and X-ray density as function Zr contents in "$Co_{0.5}Zn_{0.5}Zr_xFe_{2-x}O_4$" ferrites (x=0.0 to 1.0).

Various structural parameters like lattice constant, x-ray density, crystalline size bond length and jumping length were calculated from the XRD data. These parameters were shown in Table 1.

The lattice constant was measured by using following formula

$$a = d\sqrt{h^2 + k^2 + l^2} \quad (1)$$

where 'h k l' represent miller indices and 'd' is inter-planner spacing.

The lattice parameter was increased from 8.303 Å to 8.498 Å when zirconium concentration increases from 0.0 to 1.0. The variation in lattice parameter as function of Zr content is shown in Fig.3. The increase in lattice parameter can be explained as: Since the ionic radii of Zr^{4+} ion (0.80 Å) which is larger than the ionic radii of Fe^{3+} ion (0.67 Å) [18]. The partial

replacement of smaller iron ion by larger zirconium ion will cause the expansion of unit cell. Subsequently increasing the lattice parameter as reported by many authors [6, 10]. Hence, the shifting of diffraction peaks towards the smaller angle is caused by the replacement of Zirconium with iron. These results have very close relationship with previous published literature as reported by many authors [19, 20]. The cell volume of zirconium substituted cobalt zinc ferrite nanoparticles were also found to increase gradually with increase of zirconium concentration [10]. The lattice constant is a very important parameter determined from XRD data. It is used to find out many other properties of prepared samples such as X-ray density, average ionic radii of A-site (r_A) and average ionic radii of B-site (r_B), bond lengths A-O and B-O and jump lengths (L_A and L_B).

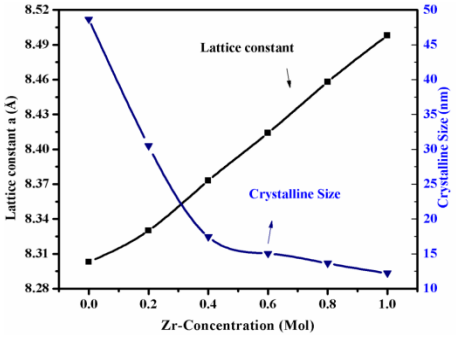

Fig. 3. The variation in lattice constant and crystalline size as function Zr contents in "$Co_{0.5}Zn_{0.5}Zr_xFe_{2-x}O_4$" spinel ferrites(x=0.0 to 1.0).

The X-ray density (ρ_x) was determined by using the value of lattice parameter. The formula used to calculate the X-ray density (ρ_x) was given as

$$\rho_x = \frac{ZM}{N_A a^3} \tag{2}$$

where 'Z' is the number of molecules per unit cell, 'M' is the molecular weight of sample, 'N_A' is the Avogadro's constant and 'a' is the lattice constant.

Fig.2 depicts the variation in bulk and X-ray densities as Zr concentration varied. Similar, increasing trend of X-ray density (ρ_x) and bulk density with increase in zirconium concentration was observed. This is due the fact that X-ray density is directly related to molar mass and the molar mass of zirconium is larger as compared to iron[19]. Also the bulk density increased due to the fact, when iron is replaced by zirconium, the overall molar mass of sample increased. Thus, X-ray density increased with increase in zirconium. This increase may also be credited due to the formation of small grain size of ferrite nanoparticles[10].

Table 1. Brief results of physical properties of $Co_{0.5}Zn_{0.5}Zr_xFe_{2-x}O_4$ (x = 0.0, 0.20, 0.40, 0.60, 0.80, 1.00): Lattice constant (a), Cell Volume(V), X-ray density (ρ_x), Average ionic radii of A-site and B-site $r_A$and r_B, Bond Lengths A-O, B-O. Jump Lengths (L_A and L_B) and crystallite size.

Composition	x = 0.00	x = 0.20	x = 0.40	x = 0.60	x = 0.80	x = 1.00
Lattice constant 'a' (Å)	8.303	8.330	8.373	8.414	8.458	8.498
Cell Volume 'V' ($Å^3$)	572.41	578.01	587.01	595.67	605.06	613.69
ρ_x (gm/cm^3)	5.519	5.629	5.703	5.778	5.843	5.914
r_A(Å)	0.448	0.453	0.463	0.472	0.481	0.490
r_B(Å)	0.726	0.732	0.743	0.754	0.764	0.774
A-O (Å)	1.798	1.803	1.813	1.822	1.831	1.840
B-O (Å)	2.076	2.082	2.093	2.104	2.114	2.124
Jump Length (L_A) (Å)	3.595	3.607	3.626	3.643	3.662	3.680
Jump Length (L_B) (Å)	2.936	2.945	2.960	2.975	2.990	3.004
D (nm)	48.66	30.50	17.45	15.04	13.64	12.22

The lattice constant is used in Standley's equations to find out the remaining parameters which are given in Table 1.

Set of Standley's Equations is given as;

Ionic radii of A-site (r_A): $r_A = (\mu-\frac{1}{4})a\sqrt{3} - r(O^{-2})$ (3)

Ionic radii of B-site (r_B) : $r_B = (\frac{5}{8} - \mu)a - r(O^{-2})$ (4)

Bond length of tetrahedral A-site: $A\text{-}O = (\mu-\frac{1}{4})a\sqrt{3}$ (5)

Bond length of octahedral B-site: $B\text{-}O = (\frac{5}{8} - \mu)a$ (6)

In above set of equations, lattice constant (a), $r(O^{-2})$ is the oxygen ion radius [1.35 Å], the oxygen ion parameter (μ) which is usually taken as $\mu = \frac{3}{8}$ for ideal spinel ferrite system[10].

The hopping lengths in A-site (L_A) and B-site (L_B) shows the distance between magnetic ions. These are determined by using following relations.

Hopping lengths in tetrahedral A-site: $L_A = a(\frac{\sqrt{3}}{4})$ (7)

Hopping lengths in octahedral B-site: $L_A = a(\frac{\sqrt{2}}{4})$ (8)

All the quantities calculated by above mentioned relations were shown in Table 1. In Table 1, it was seen that the ionic radii of A and B sites, jump length of A and B sites (L_A and L_B) and bond lengths of A and B sites increased with increase in zirconium concentration. These quantities increased due to smaller sized ionic radii are replaced by larger sized ionic radii and their settlement on octahedral B-sites and tetrahedral A-site as reported by Farid et al., 2017.

The peaks in the XRD patterns are broad, which may be due to small particle size. The crystallite size was found for each sample. The three more intense peaks of all prepared samples were chosen and crystallite size was found by using Debye Scherrer's formula[21]. Debye Scherrer's formula is given as

$$D = \frac{0.9\lambda}{\beta\cos\theta} \quad (4.9)$$

where 'D' Crystallite Size 'λ' Wavelength of incident X-ray 'θ' Bragg's diffraction angle in radians and 'β' Full width at half maximum (FWHM) value in radians.

The crystalline size trend is expressed in Fig.3. Which was found to decrease from 48.66nm to 12.22nm when substitution of zirconium increases from 0.0 to 1.0. The increase of zirconium concentration in cobalt zinc ferrite decreases grain growth due to the dissociation near the boundary of grains which hinders it movement. This will hampered the grain growth of crystal. So crystallite size of prepared Nano-ferrites decreased.

3.2. FT-IR analysis

The Fourier transform infrared spectroscopy is one of the most important technique used to obtain the IR spectrum of absorption or emission of solid, gas or liquid. The high spectral resolution data was collected over the wide spectral range. Actually the Fourier transform is a mathematical conversion process that is used to transform raw data into definite spectrum. The FT-IR analysis was used to estimate the elastic properties of ferrite nanoparticles. These elastic properties are used to determine the inter-atomic and inter-ionic forces between cations existing in ferrite nanoparticles. The elastic parameters are then used to study the thermal properties such as Debye temperature and specific heat. The measurement of these thermal properties of ferrite

samples gives the information about their suitability for industrial uses. The FT-IR spectra can also be used to guess the purity of compound.

The FT-IR technique was used to confirm the formation of spinel ferrites. The different spinel ferrites $Co_{0.5}Zn_{0.5}Zr_xFe_{2-x}O_4$ (x = 0.0, 0.2, 0.4, 0.6, 0.8, 1.0) samples were subjected to FT-IR characterization by using PerkinElmer Spectrum Two FT-IR Spectrometer. This spectrometer has capability to analyze the samples in the wave number range 400 cm^{-1} to 4000 cm^{-1}. The FT-IR spectra of $Co_{0.5}Zn_{0.5}Zr_xFe_{2-x}O_4$ is shown in the Fig.4. The FT-IR analysis was done in the frequency range 400cm^{-1} to 4000cm^{-1}. The frequency bands in the range 400-1000cm^{-1} were observed which indicated the existence of metal oxides. Moreover the FT-IR spectra confirmed the formation of spinel ferrites.

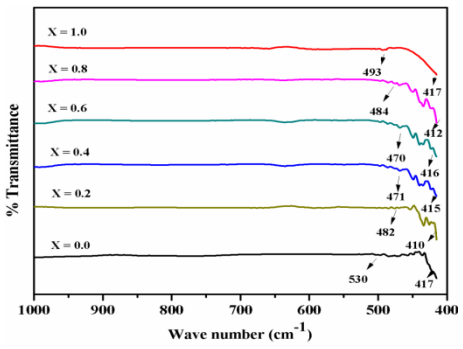

Fig. 4. FTIR spectra of "$Co_{0.5}Zn_{0.5}Zr_xFe_{2-x}O_4$" spinel ferrite (x=0.0 to 1.0).

Two major vibrations of the octahedral sites (B-O-B bonds) and the tetrahedral sites (A-O-A bonds), are observed respectively. It is well acknowledged that two main absorption bands, usually represented by υ_1 andυ_2 are typically exist in all cubic spinel ferrites[15]. The presence of these two basic bands in spectrum confirmed the formation of spinel ferrites [22, 23]. These bands are corresponds to the stretching vibrations of iron Oxide bond [13]. It also confirmed the formation of spinel ferrite nanoparticles having octahedral and tetrahedral sites [22].The corresponding values for higher band and lower band are reflected in Table 2.

The higher frequency band (υ_1) lies in the 470-530cm^{-1} which is assigned to stretching vibrations of tetrahedral (υ_1) sites (A). The lower frequency band in the range of 410cm^{-1} to 417cm^{-1} is related stretching vibrations of octahedral (υ_2) M-O groups in prepared nanoparticles [1]. The higher bands in the 660cm^{-1} to 2000cm^{-1} range were also observed. These bands are mainly occur due to the vibrations of functional groups which are present in the starting materials [13]. The higher bands is due to the stretching vibrations of H-O-H bonds which are present due to water absorbed on the surface nanoparticles [24]. These peaks at higher frequencies above the 1000cm^{-1} are attributed to some unreacted materials.

Table 2. FTIR absorption bands for "$Co_{0.5}Zn_{0.5}Zr_xFe_{2-x}O_4$" spinel ferrite (x = 0.0, 0.20, 0.40, 0.60, 0.80, 1.00).

S. No	Composition	ν_1 (cm^{-1})	ν_2 (cm^{-1})
1	$Zn_{0.5}Co_{0.5}Fe_2O_4$	530	417
2	$Zn_{0.5}Co_{0.5}Zr_{0.2}Fe_{1.8}O_4$	482	410
3	$Zn_{0.5}Co_{0.5}Zr_{0.4}Fe_{1.6}O_4$	471	415
4	$Zn_{0.5}Co_{0.5}Zr_{0.6}Fe_{1.4}O_4$	470	416
5	$Zn_{0.5}Co_{0.5}Zr_{0.8}Fe_{1.2}O_4$	484	412
6	$Zn_{0.5}Co_{0.5}ZrFeO_4$	493	417

3.3. SEM analysis

The morphological properties of $Co_{0.5}Zn_{0.5}Zr_xFe_{2-x}O_4$ (x = 0.0, 0.4, 1.0) ferrite nanoparticles were examined by using scanning electron microscope. The scanning electron

microscope gives information about the surface topography, morphology, crystallographic information and elemental compositions. Here, scanning electron microscope used to observe the shape and size of the samples under investigation. The morphological properties of$Co_{0.5}Zn_{0.5}Zr_xFe_{2-x}O_4$ (x = 0.0, 0.4, 1.0) ferrite nanoparticles were examined by using scanning electron microscope. The scanning electron microscope gives information about the surface topography, morphology, crystallographic information and elemental compositions. Here, scanning electron microscope used to observe the shape and size of the samples under investigation. The SEM micrographs of analyzed sample are shown in Fig.5.

The nanoparticles with different shapes and sizes were observed in the Fig.5. It is clear that shapes of the grain are not regular. However, most of the grain has spherical shape which confirms the formation of spinel ferrites. Many grains were found to be agglomerated. The agglomeration of grains may occur due to annealing of ferrites and interfacial surface tensions [25, 26]. The morphology of sample found be changed with substitution of zirconium. The grain boundaries of samples were found to be less clear. The zirconium ion either goes the grain boundaries or resides at Fe position. However, Fe ion has more chance to occupy tetrahedral A-site as compared to zirconium. This may be due to reason that the tetrahedral sites are very small that cannot be engaged by larger zirconium ion [27, 28]. So, zirconium ion occupies octahedral B-sites. It was also observed that average grain size decreased with increase in zirconium concentration which is in good agreement with XRD results.

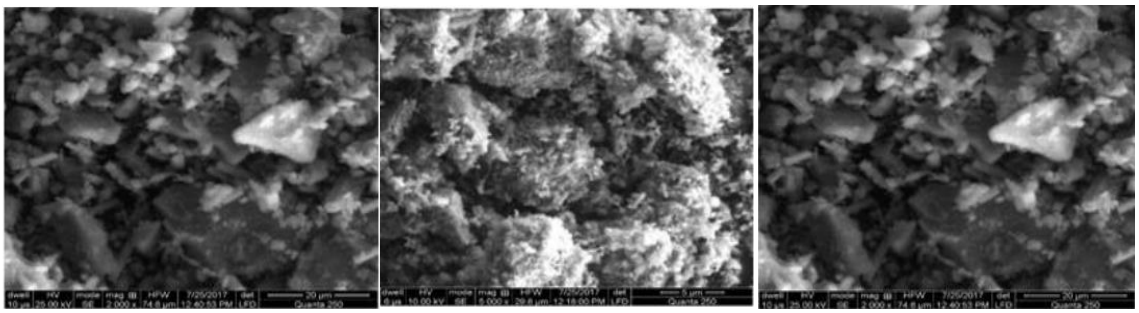

a) *b)* *c)*

Fig. 5.The scanning electron micrographs of "$Co_{0.5}Zn_{0.5}Zr_xFe_{2-x}O_4$"ferrite samples(x=0.0 to 1.0). a) x=0.4; b) x=0.0; c) x=1.0

3.4 Magnetic measurements

The M-H graph taken at room temperature for $Co_{0.5}Zn_{0.5}Zr_xFe_{2-x}O_4$ (x = 0.0, 0.2, 0.4, 0.6, 0.8 1.0) compositions as a function of external magnetic field H are shown in Fig. 6. From these loops, saturation magnetization (Ms), remanence magnetization (Mr) and coercivity (Hc) were measured. The variation in Ms, Mr and Hc values as function Zr^{+3} content is shown in Fig.7. The Mr was in small range and increased inhomogenoulsy. Whereas Ms value is maximum at x=0. The value of Hc increased inhomogenously with increased of Zr^{+3} content in CoZn-ferrite and the value of Hc was maximum when x=0.4 [29, 30];the difference between the cation concentrations with higher magnetic moment (Fe^{3+}) between two sub-lattices is higher. The magnetic moment of Fe^{3+} and Co^{2+} based on Neel's theory, which expresses the magnetization of ferrites by the magnetization difference between two sub-lattices[31, 32].As Zirconium was substituted in ferrites, the Zr^{3+} cation settled on octahedral sites and couple the magnetization of Fe^{3+} on the B-sites, this increase was the cause of the net magnetization of the B-sublattice and resulting an increase in the saturation magnetization [33, 34]. The other important magnetic parameter Hc is. The factors like porosity, grain size, particle morphology, magnetic domain size and magneto crystalline anisotropy etc control the coercivity Hc. Usually grain size has converse relation with the coercivity Hc.

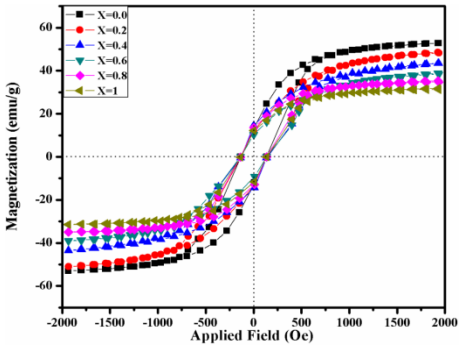

Fig. 6. Hysteresis loop for "$Co_{0.5}Zn_{0.5}Zr_xFe_{2-x}O_4$"spinel ferrite (x=0.0 to 1.0).

The larger number of domain walls likely be the result of larger grains. Consequently, the domain wall group necessitates less energy when these domain walls get magnetized or de-magnetized, in contrast to domain rotation. Decreasing grain sizes also decreases the number walls and wall movement decreases.

Table 3. Various magnetic parametersfor"$Co_{0.5}Zn_{0.5}Zr_xFe_{2-x}O_4$" spinel ferrite (x = 0.0, 0.20, 0.40, 0.60, 0.80, 1.00).

Magnetic Parameters In	x=0	x=0.2	x=0.4	x=0.6	x=0.8	x=1
Coercivity (Hc)/Oe	137.60	142.95	144.14	137.58	138.14	136.8
Magnetization (Ms) (emu/g)	52.8	48.6	43.59	38.22	34.56	31.83
Retentivity (Mr) (emu/g)	13.5	11.98	14.59	10.16	13.72	12.19
Squareness Ratio (Mr/Ms)	0.2557	0.2465	0.3347	0.2658	0.3970	0.3829
Anisotropy constant (J/m^3)	0.0046	0.0044	0.004	0.0033	0.003	0.0027

As result, samples having smaller grains are anticipated to have larger coercivity, and vice versa. This general reason may be the cause for the reduce in coercivity of the different compositions of the ferrites [10, 35].It can be noticed the smaller value of coercivity Hc of the ferrite samples, there by indicate these materials are the soft magnetic materials. Furthermore, with the replacement of Zr^{3+} ions, Hc of the samples inhomogeneous trends. But overall decrease in the Hc value. In $Co_{0.5}Zn_{0.5}Zr_xFe_{2-x}O_4$, the Fe^{3+} ions stay on tetrahedral as well as on the octahedral sites, while Zr^{3+} ions reside on the octahedral site due to the larger ionic radii as compared to Fe^{3+} ions. So there is a smaller chance of Zr^{3+} to reside on tetrahedral site[36]. As Zr^{3+} is non-magnetic, consequently magnetic moments on the octahedral site is less than magnetic moments on tetrahedral site and it has no more impact in magnetization of spinel ferrites. This can be one of the reasons for the decrease in magnetization [37].

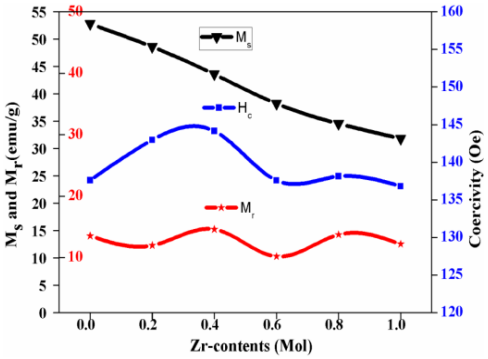

Fig. 6. The variation in Ms, Mr and Hc values as function Zr content in "$Co_{0.5}Zn_{0.5}Zr_xFe_{2-x}O_4$" spinel ferrites (x=0.0 to 1.0).

The other factor of decrease in saturation magnetization may be due to the transfer of ferric ions from B-sites to A-sites[38]. In this current work, an improved 'Ms' saturation magnetization (52.8 emu/g) and 'Hc' coercivity values (114.14Oe) have been obtained. The value of Hc is low, so synthesized $Co_{0.5}Zn_{0.5}Zr_xFe_{2-x}O_4$ ferrites is suitable for low core losses on transformers.

4. Conclusions

Zirconium substituted spinel ferrites with chemical composition$Co_{0.5}Zn_{0.5}Zr_xFe_{2-x}O_4$ (x = 0.0, 0.2, 0.4, 0.6, 0.8 1.0) have been successfully synthesized by co-precipitation method. X-ray diffraction analysis depicted that spinel ferrites with single phase are obtained in nano regime. Different parameters like grain size, lattice constant and x-ray densities are obtained from XRD data. FTIR analysis confirmed that the existent of metal oxide at tetrahedral site and octahedral sites. Those are characteristics of the spinel structure. Morphological analysis confirms the formation of inhomogenously distributed.

At room temperature the VSM measurement indicated that the effect of the applied magnetic field intensity upon the magnetic properties of the synthesized powder intensifies the remanence magnetization by 13.72emu/g and the coercivity by 144.14Oe as an effect of the applied alternative magnetic field. Anisotropy constant value are small that indicate the isotropic nature of the magnetic powder. Due to low coercivity and sufficient value of Ms ranging 31 to 52emu/g indicate suitability of material for low core losses on transformers.

Acknowledgement

We are thankful to Government College University Faisalabad, Pakistan and ORIC office, Balochistan University of Information Technology, Engineering and Management Sciences (BUITEMS), Quetta Pakistan providing necessary facilities.

References

[1] S. Bhukal, S. Bansal, S. Singhal, Journal of Molecular Structure **1059**,150 (2014).
[2] M.A. Ahmed, N. Okasha, M. Gabal, Materials Chemistry and Physics**83**,107 (2004).
[3] Z.A. Gilani, M.S. Shifa, M.A. Khan, M.N. Anjum, M.N. Usmani, R. Ali, M.F. Warsi, Ceramics International, (2017).
[4] A. Ghafoor, M.A. Khan, M.U. Islam, Z.A. Gilani, A. Manzoor, H.M. Khan, I. Ali, M.F. Warsi, Ceramics International **42**,14252 (2016).
[5] M. Ben Ali, K. El Maalam, H. El Moussaoui, O. Mounkachi, M. Hamedoun, R. Masrour,

E.K. Hlil, A. Benyoussef, Journal of Magnetism and Magnetic Materials **398**,20 (2016).
[6] R. Ali, M.A. Khan, A. Manzoor, M. Shahid, S. Haider, A.S. Malik, M. Sher, I. Shakir, M. Farooq Warsi, Journal of Magnetism and Magnetic Materials **429**,142 (2017).
[7] I.H. Gul, A. Maqsood, Journal of Alloys and Compounds **465**,227 (2008).
[8] S. Bhukal, Shivali, S. Singhal, Materials Science in Semiconductor Processing **26**,467 (2014).
[9] S. Bhukal, S. Bansal, S. Singhal, Physica B: Condensed Matter **445**,48 (2014).
[10] H.M. Tahir Farid, I. Ahmad, K.A. Bhatti, I. Ali, S.M. Ramay, A. Mahmood, Ceramics International**43**,7253 (2017).
[11] M.A. Gabal, A.A. Al-Juaid, S.M. Al-Rashed, M.A. Hussein, F. Al-Marzouki, Journal of Magnetism and Magnetic Materials**426**,670 (2017).
[12] P. Thakur, R. Sharma, V. Sharma, P.B. Barman, M. Kumar, D. Barman, S. C. Katyal, P. Sharma, Journal of Magnetism and Magnetic Materials **432**,208 (2017).
[13] S. Torkian, A. Ghasemi, R.S. Razavi, Ceramics International**43**,6987 (2017).
[14] S. Urcia-Romero, O. Perales-Pérez, G. Gutiérrez, Journal of Applied Physics **107**,09A508 (2010).
[15] N. Murali, S.J. Margarette, G.P. Kumar, B. Sailaja, S.Y. Mulushoa, P. Himakar, B.K. Babu, V. Veeraiah, Physica B: Condensed Matter **522**,1 (2017).
[16] H. Sozeri, Z. Durmus, A. Baykal, Materials Research Bulletin **47**,2442 (2012).
[17] I. Gul, A. Abbasi, F. Amin, M. Anis-ur-Rehman, Journal of Magnetism and Magnetic Materials **311**,494 (2007).
[18] K.J. Standley, Oxide magnetic materials, Oxford University Press1972.
[19] R. Ali, M.A. Khan, A. Manzoor, M. Shahid, S. Haider, A.S. Malik, M. Sher, I. Shakir, M. FarooqWarsi, Journal of Magnetism and Magnetic Materials **429**,142 (2017).
[20] I. Ali, M. Islam, M. Ishaque, H.M. Khan, M.N. Ashiq, M. Rana, Journal of Magnetism and Magnetic Materials **324**,3773 (2012).
[21] B.D. Cullity, S.R. Stock, Elements of X-ray Diffraction, Pearson Education2014.
[22] T.R. Tatarchuk, N.D. Paliychuk, M. Bououdina, B. Al-Najar, M. Pacia, W. Macyk, A. Shyichuk, Journal of Alloys and Compounds**731**,1256 (2018).
[23] S. Amiri, H. Shokrollahi, Journal of Magnetism and Magnetic Materials **345**,18 (2013).
[24] M.K. Lima-Tenório, L.A. Oliveira, M.R. Guilherme, E.T. Tenório-Neto, M.F. Silva, D.M. Fernandes, A.A. Hechenleitner, E.A. Pineda, Materials Letters**195**,151 (2017).
[25] M. Sundararajan, L.J. Kennedy, Journal of Environmental Chemical Engineering **5**,4075 (2017).
[26] R.A. Pawar, S.S. Desai, S.M. Patange, S.S. Jadhav, K. M. Jadhav, Physica B: Condensed Matter **510**,74 (2017).
[27] F. Moeinpour, A. Khojastehnezhad, Arabian Journal of Chemistry **10**,S3468 (2017).
[28] M. Asif Iqbal, M.-U. Islam, M.N. Ashiq, I. Ali, A. Iftikhar, H.M. Khan, Journal of Alloys and Compounds **579**,181 (2013).
[29] M.A. Khan, M.U. Islam, M. Ishaque, I.Z. Rahman, Ceramics International **37**,2519 (2011).
[30] Q. Lin, G. Yuan, Y. He, L. Wang, J. Dong, Y. Yu, Materials & Design **78**,80 (2015).
[31] M.S. Samadi, H. Shokrollahi, A. Zamanian, Materials Chemistry and Physics **215**,355 (2018).
[32] Y. Yafet, C. Kittel, Physical Review **87**,290 (1952).
[33] I. Soibam, S. Phanjoubam, C. Prakash, Journal of Magnetism and Magnetic Materials **321**, 2779 (2009).
[34] V.S. Sawant, K.Y. Rajpure, Journal of Magnetism and Magnetic Materials **382**,152 (2015).
[35] A.K.M. Akther Hossain, M.A. Rahman, S.F.U. Farhad, B. Vilquin, H. Tanaka, Physica B: Condensed Matter **406**,1506 (2011).
[36] Y. Zhou, X. Wu, W. Wu, X. Huang, W. Chen, Y. Tian, D. He, Materials Science in Semiconductor Processing **41**,162 (2016).
[37] V. Jagadeesha Angadi, B. Rudraswamy, K. Sadhana, S.R. Murthy, K. Praveena, Journal of Alloys and Compounds **656**,5 (2016).
[38] R. Ali, A. Mahmood, M.A. Khan, A.H. Chughtai, M. Shahid, I. Shakir, M.F. Warsi, Journal of Alloys and Compounds **584**,363 (2014).